

---

PHYSICOCHEMICAL PROCESSES  
AT THE INTERFACES

---

## Hydrogen Production on Aluminum in Alkaline Media

S. M. Abd El Haleem<sup>a</sup>, S. Abd El Wanees<sup>a,b,\*</sup>, and A. Farouk<sup>a</sup>

<sup>a</sup> Chemistry Department, Faculty of Science, Zagazig University, Zagazig, Egypt

<sup>b</sup> University College of Umluj, Umluj, Tabuk University, Tabuk, Kingdom of Saudi Arabia

\*e-mail: s\_wanees@yahoo.com

Received January 29, 2021; revised May 3, 2021; accepted May 10, 2021

**Abstract**—The corrosion behavior and hydrogen generation on aluminum in NaOH solutions are followed up using different techniques. The rates of Al<sub>2</sub>O<sub>3</sub> film destruction, metal dissolution, and hydrogen gas production are dependent on the alkali amount and the solution temperature. The existence of two capacitive semi-circles at high and low frequencies confirm the charge transfer process on the metal surface. The existence of an inductive loop at intermediate frequencies emphasizes the surface charge due to the building up of oxide film at the Al/Al<sub>2</sub>O<sub>3</sub> interface. Low values of free energy of activation of these processes  $E_a$  indicate that these processes are controlled by a diffusion step. The positive values of  $\Delta H_a$  reflect the endothermic nature of the activation processes, while the negative values of  $\Delta S_a$  indicate a decreased disordering of a dissociation step.

**Keywords:** aluminum, corrosion rate, H<sub>2</sub> production, impedance, thermodynamic functions, gravimetry, gasometry, galvanostatic polarization

**DOI:** 10.1134/S2070205121050099

### INTRODUCTION

Production of hydrogen gas by chemical processes, always starting from hydrogen-containing compounds, plays a favorable role in the recent developments of energy technologies. Another way for the production of H<sub>2</sub> is the reduction of H<sub>2</sub>O employing aluminum and/or some of Al/alloys [1–3]. Due to the corresponding high energy density and high negative redox potential of these materials, aluminum is considered as a superior conversion factor susceptible for generating H<sub>2</sub> upon reaction with H<sub>2</sub>O in a corrosion process [4, 5]. Although the reaction of Al with H<sub>2</sub>O is thermodynamically feasible, it does not precede continually due to the existence of a cohesive and adherent film of aluminum oxide [6–8]. This oxide film prohibits H<sub>2</sub>O to be in an immediate approach with the metal surface.

The solubility of the aluminum oxide layer is frivolous in aqueous neutral solutions; however, intensive dissolution is noticed in both acidic and alkaline aqueous solutions [9–14]. Alkaline corrosion of Al is technically necessary as specially noted in the anodic reaction of the aluminum/air batteries, which are sophisticated as power sources for electric vehicle propulsion [15–20]. The corrosion resistance of aluminum, under these conditions, should be controlled to optimize the maximum execution of such batteries. The corrosion of Al in alkaline media is supposed to take place in two conjugated electron transfer steps involving the formation of Al<sup>3+</sup> and generation of H<sub>2</sub> gas, succes-

sively. The rate of Al corrosion depends on many factors like OH<sup>-</sup> ion concentration and the quantity of Al(OH)<sub>4</sub> in solution [21–23]. The dissolution of Al takes place through an oxide film via ionic migration through the oxide film pursued by a dissolution-step at the oxide/electrolyte interface [24, 25]. However, Macdonald et al. proposed that, in alkaline media, the dissolution of aluminum occurs through the step-wise movement of OH<sup>-</sup> ions to the surface Al atoms to form meta aluminate species, Al(OH)<sub>4</sub> [26]. Other studies indicated the formation of AlH<sub>3</sub> as an intermediate during the dissolution of Al in alkaline solution [27–29].

The present investigation aims to study the kinetics of destruction of the surface Al<sub>2</sub>O<sub>3</sub> film, dissolution of the metal, and the subsequent generation of H<sub>2</sub> gas in NaOH solutions. Thermodynamics of these processes are evaluated and discussed under different experimental conditions involving chemical and electrochemical techniques such as potentiometric, gravimetric, gasometric, galvanostatic polarization, and impedance techniques, as well as surface examination.

### 2. EXPERIMENTAL

#### 2.1. Materials and Methods

The Aluminum Company of Egypt provided the used aluminum samples. The procedure of metal preparation and measurements were analogous to that declared elsewhere [9, 10]. For gravimetric, gasomet-

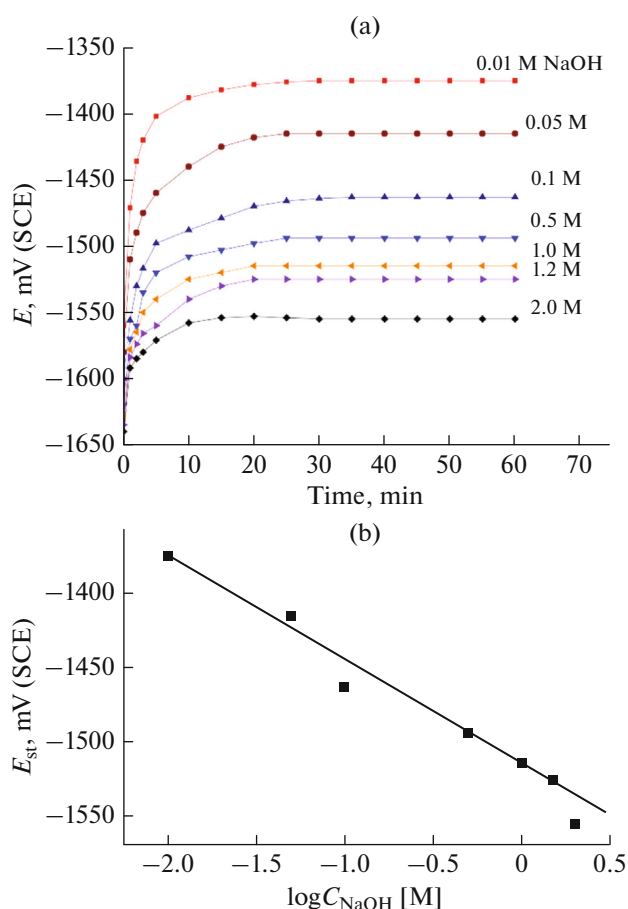


**Fig. 1.** (a) Variation of the open circuit potential  $E$  of Al electrode with immersion time in solutions of different concentrations of NaOH; (b) Variation of the steady-state potential with the logarithm of NaOH concentration.

ric, and thermometric measurements, Al specimens of  $55 \times 12 \times 3.1$  mm were prepared. The working electrode (WE) for potentiometry and electrochemical measurements, was also prepared from a bar of pure Al metal. This bar was embedded inside a Teflon rod with an exposed contact surface area of  $0.35 \text{ cm}^2$ . Before any experiment, the sample surface was cleaned by polishing with emery papers (various grades) and rinsed by distilled water, followed by acetone. NaOH solution was prepared by taking the accurate weight of the pure solid, dissolved in distilled water, and then standardized against standard HCl solution. Experiments were always done at  $25 \pm 1^\circ\text{C}$ , except those carried out at different temperatures, an air thermostat was used.

### 2.2. Potentiometric Study

The change in the Al electrode potential, open-circuit potential OCP was followed relative to a saturated calomel electrode (SCE) using a Wenking potentiometer, type PPT 70. The final stable potential  $E_{st}$  was

taken when the OCP did not change by  $\pm 1 \text{ mV}/5 \text{ min}$ . Each set of the run was done in a new solution and a polished Al electrode.

### 2.3. Gravimetric and Hydrogen Gas Generation Measurements

Weight loss experiments for Al in NaOH solutions were carried out using rectangular Al coupons having the same purity as Al rods. The Al samples and the WE were polished, washed and dried, weighed, and then submerged in 0.25 L of the examined solution for the desired period. Following this, the samples were rinsed with distilled water, dried, and re-weighed. The loss in weight ( $\Delta W$ ) was made in duplicate, and the average value was taken. The extreme standard deviation in  $\Delta W$ , ( $\text{mg cm}^{-2}$ ), was  $\pm 0.5\%$ . The corrosion reaction rate  $R_{\text{corr}}$  in  $\text{mg}/\text{cm}^2/\text{h}$  can be estimated from the equation [9, 10]:

$$R_{\text{corr}} = \left( \frac{\Delta W}{\text{area} \times \text{time}} \right). \quad (1)$$

The gasometric reaction for  $\text{H}_2$  generation on Al in NaOH was carried out in a suitable apparatus. The vessel and the experimental procedure were described early [9, 10, 29, 30]. The corrosion reaction rate,  $R'_{\text{corr}}$ , was assessed from the volume-time plots of the evolved  $\text{H}_2$ .

### 2.4. Electrochemical Studies

The electrolytic cell and the different electrodes were utilized as shown early [9, 10, 30, 31]. Al rod, Pt sheet, and SCE were employed as a WE, counter, and reference electrodes successively. Before any test, the Al electrode was inundated in the investigated solution until the potential approaches the  $E_{st}$  value. Galvanostatic potential-current curves were constructed for each of the cathodic and anodic polarization runs. The EIS experiments were done utilizing potentiostat/galvanostat/ZRA, Gamry, USA. The applied frequency range was varied between 0.1 Hz–100 kHz with an AC amplitude of 5 mV [32, 33].

## RESULTS AND DISCUSSION

### 3.1. Potentiometric Study

The attitude of the Al electrode inundated in NaOH of different concentrations was explained by measuring the OCP as a function of the inundation time  $t$  till steady-state potential was attained. The data of Fig. 1a explain the behavior of the Al electrode in NaOH solutions of concentrations varying between  $1 \times 10^{-2}$  and 2.0 M. As could be shown from the data of the curves,  $E_{st}$  is attained from the more negative direction and become more active the higher the alkali strength.

Figure 1b represents the divergence of  $E_{st}$  with the NaOH concentration,  $\log C_{NaOH}$ , which give a straight-line relation according to [9, 10, 34]:

$$E_{st} = \phi - \psi \log C_{NaOH}, \quad (2)$$

where  $\phi$  and  $\psi$  are constants. The intercept  $\phi$  exemplifies the  $E_{st}$  at 1.0 M NaOH, which compensates  $-1515$  mV and the slope  $\psi$  equals  $73$  mV/ $\log C_{OH^-}$ .

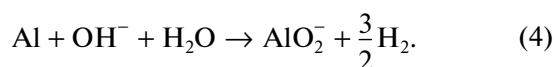
The positive shift of the OCP  $E$  of the Al metal when immersed in NaOH solutions of various concentrations denotes that the pre-inundation  $Al_2O_3$  film on the aluminum surface is not adequate to realize complete passivity [36] and that recovery and intensification of the film continue till this state of affairs is accomplished [9, 10, 37]. In our study in such a situation, the reduction of oxygen reaction of the corrosion process [38, 39]. The necessary electrons for the oxygen reduction are supplied from the oxidation of Al atoms entering the passive phase,

$Al_2O_3$ :



This reaction takes place under the impact of an anodic current that polarizes the Al metal and shifts the  $E$  into the noble direction.

The shift of  $E_{st}$  values into the active direction upon increasing the concentration of NaOH, Figs. 1a, 1b, could be ascribed to the partial dissolution of the  $Al_2O_3$  layer and subsequent increase in the corrosion rate of Al in NaOH medium. The corrosion reaction of Al in alkaline medium greatly increases with increasing pH of the solution, unlike iron and steel, which retain corrosion resistance. The reason for this difference is that  $Al^{3+}$  is readily complexed by  $OH^-$ , forming  $AlO_2^-$ , according to the reaction:



This reaction proceeds rapidly at room temperature, whereas for iron and steel, similar reactions forming  $FeO_2^-$  and  $FeO_2^{2-}$  require concentrated alkali and high temperatures [40]. The curves of Fig 2a depict the variation of the OCP  $E$  of Al electrode with the inundation time  $t$  in naturally aerated 2.0 M NaOH solutions, at various temperatures (15–55°C). The data of Fig. 2a shows that upon increasing the temperature, the value of  $E_{st}$  is also attained from the negative direction to take more negative values with an increase in the solution temperature, Fig. 2b. However, the increase in the solution temperature promotes the rate of oxide film destruction and/or reduces the rate of oxide film growth [41, 42], causes the promotion of Al dissolution. The steady-state potential is shifted into the active direction by a rate of 1.24 mV/degree. Zumdahl believed that increasing the temperature reduces the solution viscosity, followed

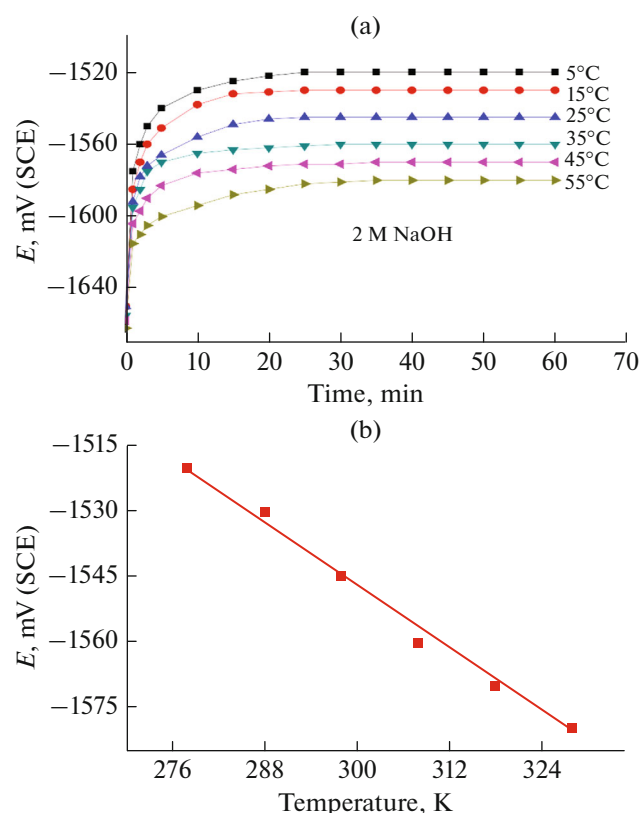


Fig. 2. (a) Variation of the open circuit potential,  $E$ , of Al electrode with immersion time in 2 M NaOH, at different temperatures, (b) Variation of the steady-state potential with solution temperature.

by a subsequent rise in ions' mobility, enhancing the dissolution reactions [43].

### 3.2. Gravimetric and Gasometric Studies

Figure 3a depicts the divergence of the rate of dissolution of Al,  $R_{corr}$ ,  $g\ cm^{-2}\ h^{-1}$ , with the  $\log C_{NaOH}$  of different NaOH solutions, as determined from weight loss measurements. As is noted from this figure, the values of  $R_{corr}$  increase linearly with increasing the alkali concentration, Table 1, according to the straight-line relation:

Rate of corrosion,  $R_{corr} = \phi_1 + \psi_1 \log C_{NaOH}$ , (5) where  $\phi_1$  and  $\psi_1$  are constants. The constant  $\phi_1$  represents the rate of corrosion,  $R_{corr}$ , of Al in 1.0 M NaOH solution and amounts to  $0.0143\ g\ cm^{-2}\ h^{-1}$  and the constant  $\psi_1$  equals  $0.016\ g\ cm^{-2}\ h^{-1}/decade$  of unit concentration.

The influence of temperature on the rate of dissolution of Al samples after one-hour immersion in 2.0 M NaOH solution, as evident from the loss in weight measurements, was studied within the temperature range 15–55°C, as shown in Fig. 3b and Table 2. As could be detected from this figure, the dis-

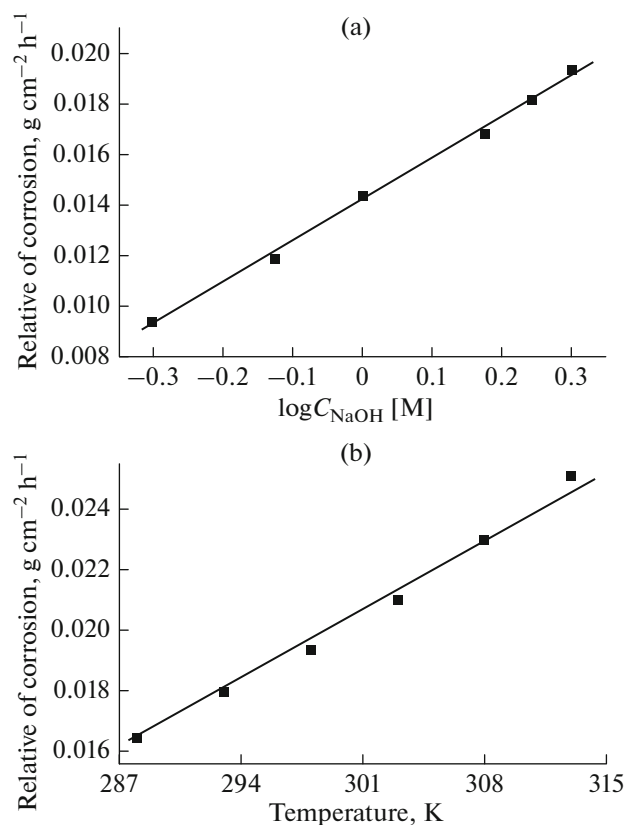


**Fig. 3.** (a) Variation of the rate of corrosion  $R_{\text{corr}}$  (g cm<sup>-2</sup> h<sup>-1</sup>) with the logarithm of NaOH concentration as evident from weigh loss measurements. (b) Variation of the rate of corrosion  $R_{\text{corr}}$  (g cm<sup>-2</sup> h<sup>-1</sup>) of Al electrode with the temperature.

solution rate of Al in 2.0 M NaOH increases linearly with the solution temperature, giving rise to a temperature coefficient of 0.332 mg cm<sup>-2</sup> h<sup>-1</sup> K<sup>-1</sup>.

Aluminum readily dissolves in NaOH with the generation of H<sub>2</sub> gas according to the overall reaction:



The rate of H<sub>2</sub> gas generation corresponds consequently to the rate of metal dissolution according to

**Table 1.** Values of corrosion rate of Al as function of concentrations of NaOH, using weight loss and hydrogen gas generation measurements, at 25°C

Concentration of NaOH, M	Rate of corrosion,	
	$R_{\text{corr}}$ , g/cm <sup>2</sup> h	$R'_{\text{corr}}$ , mL/cm <sup>2</sup> min
0.50 M	0.0094	0.233
0.75 M	0.0119	0.296
1.00 M	0.0143	0.351
1.50 M	0.0168	0.422
1.75 M	0.0182	0.471
2.00 M	0.0193	0.490

reaction 6. In the present investigation, the rate of dissolution of Al  $R'_{\text{corr}}$  in different concentrations of NaOH solutions was followed by measuring the volume of the evolved H<sub>2</sub> gas  $V_{\text{ml}}$ . The data of Fig. 4a depicts the divergence in the volume ( $V$ ) of the evolved H<sub>2</sub>, in mL/cm<sup>2</sup> with the inundation time  $t$  in minutes for Al immersed in NaOH solutions of various concentrations (0.5–2.0 M), at 25°C. This figure shows that the measured  $V_{\text{ml}}$  on Al surface depends on the alkali concentration and increases continuously and linearly with time following the relation [9, 10]:

$$V = R_s t, \quad (7)$$

where  $V$  is the volume of H<sub>2</sub> in mL per square centimeter of the metal surface,  $t$  is the time in minutes and  $R_s$  is the specific rate constant of the dissolution process.

The slope of the straight lines of Fig. 4a is considered as a value of the rate of dissolution of Al in NaOH solution  $R'_{\text{corr}}$ , Table 1. It is quite clear that the rates of free Al dissolution and hydrogen gas generation rise with increasing the alkali concentration. The influence of temperature on the  $V_{\text{ml}}$  of the evolved H<sub>2</sub> for Al inundated in 2.0 M NaOH solution is indicated in Fig. 4b. As could be shown from this figure, on raising the temperature, the volume of H<sub>2</sub> gas generated increases, and consequently, the rate of Al dissolution,  $R'_{\text{corr}}$  increases as shown in Table 2.

### 3.3. Galvanostatic Polarization Study

Figure 5A shows the anodic-cathodic curves,  $E$ -log  $I$ , of Al in NaOH solutions of concentrations varying between  $1 \times 10^{-2}$  M and 2.0 M, at 25°C, under galvanostatic polarization conditions. It is evident from the curves of this figure that the concentration of NaOH has marked effects on the anodic/cathodic polarization curves. First of all, the  $E$ -log  $I$  polarization curves of Fig. 5a are characterized by a limiting anodic current  $I_L$ . As could be seen from the data of Fig. 5a, the limiting anodic dissolution current  $I_L$  increases markedly with raising the alkali concentration due to high rates of corrosion. Figure 5b shows the divergence of the limiting current density  $I_L$  versus NaOH concentration. A straight-line relation between the two variables is obtained. This relation confirms that the corrosion of Al in NaOH solution occurs under diffusion control [44, 45]. The relationship between the limiting current density  $I_L$  and the diffusion coefficient  $D$  could be written as [46]:

$$I_L = DZFC/\delta, \quad (8)$$

where  $Z$  is the number of e<sup>-</sup> involved in the dissolution reaction,  $F$  is Faraday constant,  $C$  is the concentration of the electro-active species, and  $\delta$  is the thickness of the diffusion film. Assuming that the  $\delta$  is constant, then the increase in the limiting current density  $I_L$  with rising the NaOH strength could be attributed to the

increase of the value of the diffusion coefficient,  $D$ . In Table 3, the electrochemical corrosion parameters  $E_{\text{corr}}$ ,  $i_{\text{corr}}$ ,  $B_a$ ,  $B_c$  and the polarization resistance,  $R_p$  are depicted as a function of NaOH concentration. The  $R_p$  is determined from plotting the potential  $E$  of the non-linear sections of the  $E$ -log  $I$  curves of Fig. 5A versus the current density  $i$ . Straight-line relationships are obtained (not shown) with slopes ( $E/I$ ), which correspond to the polarization resistance values  $R_p$  [47].

Analysis of the polarization curves of Fig. 5a and the data of Table 3 manifests that increasing the concentration of NaOH causes the displacement of both the anodic and cathodic polarization curves with the consequent marked decrease in the values of  $B_a$  and  $B_c$ . The corrosion potential  $E_{\text{corr}}$  becomes more active with increasing the alkali concentration with a corresponding increase in the corrosion current density  $i_{\text{corr}}$ . Both effects denote the marked increase in the rates of dissolution of Al and the  $H_2$  gas production with increasing the NaOH concentration. This is further confirmed with a marked decrease in the values of polarization resistance  $R_p$ .

The dissolution reaction of Al cannot be considered as an individual step. It comprises two complemented electron transfer reactions, the reaction between Al and  $Al^{3+}$  and the other between  $H_2O$  and  $H_2$ . The rate of destruction depends, consequently, on many variables involving  $OH^-$  ion concentration and the amount of  $Al(OH)_4$  in the solution [44]. Some authors thought that the dissolution of Al in alkaline media takes place through an oxide film via ionic migration through the oxide film followed by dissolution at the oxide/electrolyte interface [24, 25].

The influence of temperature on the galvanostatic polarization of Al in 2.0 M NaOH solutions is shown in Fig. 6. The different corrosion characters like  $E_{\text{corr}}$ ,  $i_{\text{corr}}$ ,  $B_a$ ,  $B_c$ , and  $R_p$  for Al in NaOH are depicted in Table 4. The obtained data shows that upon raising the solution temperature, the corrosion potential is displaced into the negative direction, and the corrosion current density,  $i_{\text{corr}}$  is markedly raised while the polarization resistance  $R_p$  is significantly decreased. These data could be explained based on increasing the rates of Al dissolution and hydrogen gas production on raising the temperature.

### 3.4. EIS Study

The electrochemical impedance technique was utilized to examine the corrosion attitude of Al in NaOH solutions of various concentrations. The Nyquist plots in Figs. 7a, 7b depicted the impedance data. In all examined solutions, the impedance curves of Al in NaOH show a major capacitive semicircle at high frequencies, a small inductive loop at medium frequencies, pursued by a tiny semicircle at low frequencies [48, 52]. Such behavior confirms that the dissolution pro-

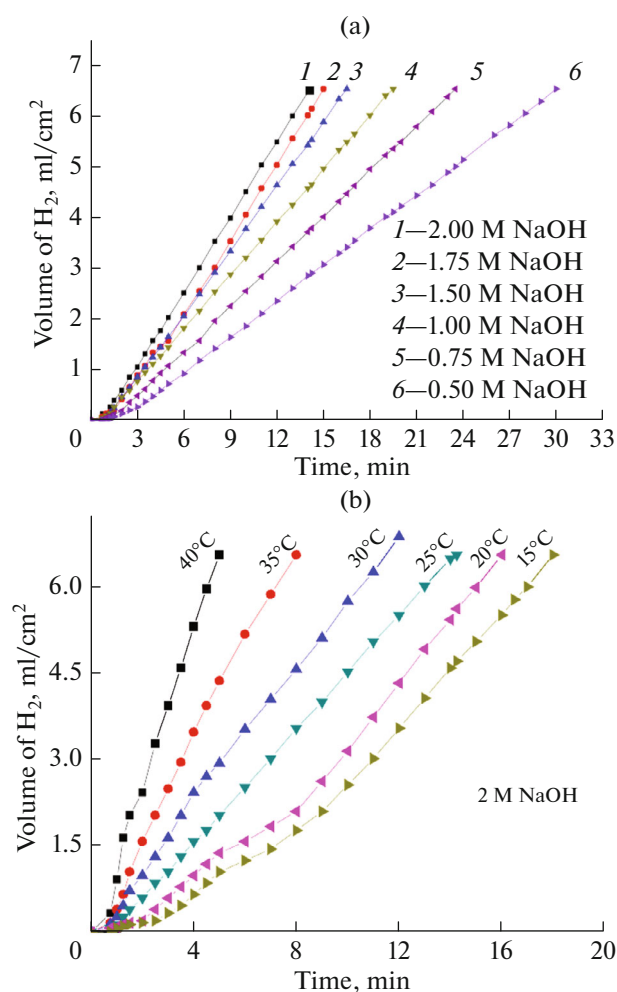


**Fig. 4.** (a) Variation of the volume of  $H_2$  gas evolved, in  $mL/cm^2$ , on Al surface in NaOH solutions of concentrations ranging from 0.5 to 2 M, with immersion time in minutes. (b) Effect of temperature on the volume of  $H_2$  gas evolved,  $mL/cm^2$ , on Al surface, in 2 M NaOH solution, with immersion time, in minutes.

cess of Al in NaOH solutions dominances by a charge transfer step [53]. The presence of depressed semicircles of these plots suggests the allocation of capacitance to be due to the inhomogeneous nature of the

**Table 2.** Rates of corrosion of Al in 2 M NaOH at different temperatures, using gravimetric and gasometric measurements

Temperature, K	Rate of corrosion	
	$R_{\text{corr}}$ , $g/cm^2 h$	$R'_{\text{corr}}$ , $mL/cm^2 min$
288	0.0165	0.420
293	0.0179	0.482
298	0.0193	0.570
303	0.0200	0.676
308	0.0230	0.816
313	0.0251	1.003

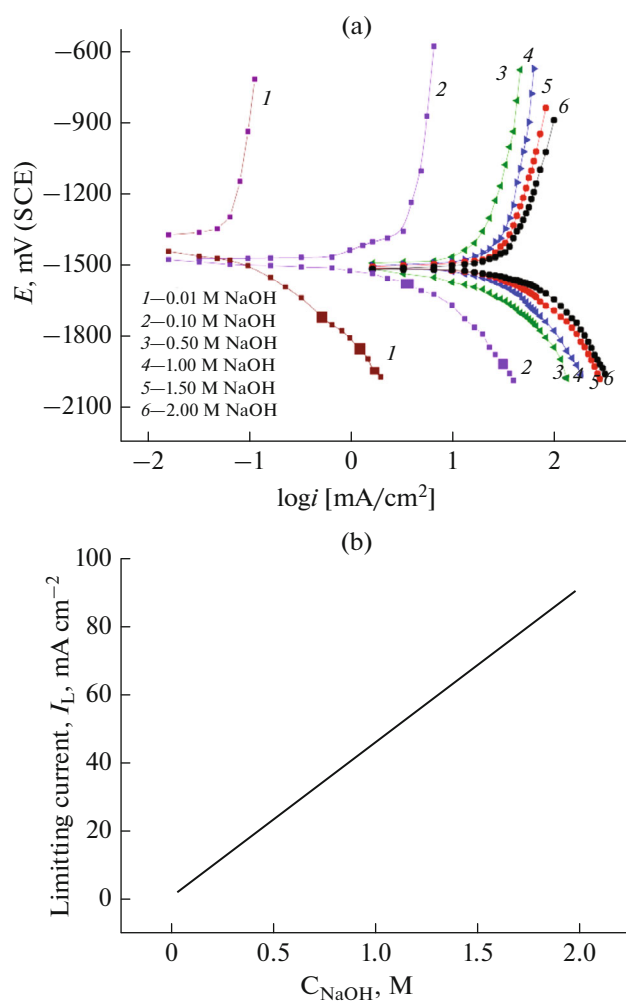


**Fig. 5.** (a) Anodic and cathodic  $E$ - $\log i$  curves of Al in solutions of NaOH of different concentrations. (b) Variation of the limiting current density with NaOH concentration.

investigated Al surface [54]. It is noteworthy to note that the high frequencies capacitive loop could be referred to as the existence of a protective oxide layer covering the metal surface [50]. This capacitive loop corresponds to an interfacial effect, particularly, the oxidation process of Al at the metal/oxide/solution interface [55]. This process produces a monovalent  $\text{Al}^+$  ion at the surface

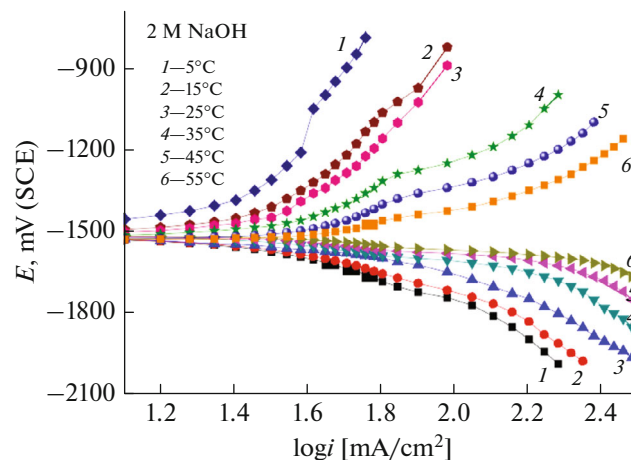


**Fig. 6.** Anodic and cathodic  $E$ - $\log i$  curves of the Al electrode in 2 M NaOH solution, at different temperatures.

of the metal oxide that could be migrated via the oxide/solution interface with the formation of trivalent ions,  $\text{Al}^{3+}$ . Also, the oxyanions  $\text{OH}^-$  or  $\text{O}^{2-}$  ions could be formed at the oxide film/solution interface as possible complemented cathodic reactions. The second capacitive semicircle at low frequencies could be related to the simultaneous redox  $\text{Al}^+ - \text{Al}^{3+}$  process [54]. However, the low frequencies inductive loop are probably related to the relaxation process due to the processes of adsorption and incorporation of the  $\text{OH}^-$  ions into the oxide layer [56]. Analogous results were obtained on studying the impedance behavior of Al in 2.0 M and 4.0 M NaOH solutions [52, 57].

The fact that all the three capacitive semicircles obtained, in the present investigation, are characteristics by the existence of a single loop could be related either to the overlapping of the loops of processes taking place or to the assumption that one approach dominates at the expense of the others [58]. It is to be noted further that the high-frequency capacitive loop, reported in the present study, and with other authors, depends on the nature of the oxide film formed on the metal surface.

The suggested equivalent circuit depicted in Fig. 8 was utilized to analyze the impedance data of Al in

**Table 3.** Electrochemical polarization parameters, of corrosion of Al in different concentrations of NaOH solutions

Concentration of NaOH, M	$-E_{\text{corr}}$ , mV/SCE	$I_{\text{corr}}$ , mA/cm <sup>2</sup>	$\beta_a$ , mV/SCE	$\beta_c$ , mV/SCE	$R_p$ , $\Omega$ cm <sup>2</sup>
0.01 M	1405	0.06	877	680	1219
0.10 M	1411	2.21	762	520	242.5
0.50 M	1465	7.62	683	440	27.15
1.00 M	1495	15.83	530	415	23.94
1.50 M	1503	21.74	464	389	11.97
2.00 M	1510	29.38	292	254	08.91

NaOH solutions. A three-time constant equivalent circuit was applied to fit some of the experimental results. The parameters extracted from the fitting of the experimental results are the solution resistance and the resistance of the two different oxide layers formed on the Al surface ( $R_1$  and  $R_2$ ). Meanwhile, the  $R_{ct}$  resistance depicts the bare Al interface with constant phase elements (CPE1, CPE2, and CPE3). The fitted results of  $R_1$ ,  $R_2$ , and  $R_{ct}$ , the admittance of the constant phase elements ( $Y_1$ ,  $Y_2$ , and  $Y_3$ ) and the inductor ( $L_1$ ), are tabulated in Table 5.

The obtained data signalize that the constant phase element,  $Y^\circ$ , decreased as the resistance values increased with increasing the thickness of the protective oxide film on the metal/solution interface. Both values depend on the strength of the NaOH solution.

The polarization resistance  $R_p$  and double layer capacitance  $C_{dl}$  could be estimated from the following equations:

$$R_p = R_L + R_{ct} + R_1 + R_2, \quad (9)$$

$$C_{dl} = n \sqrt{\frac{Q}{R^{(\alpha-1)}}} (\alpha - 1), \quad (10)$$

where  $Q$  is the CPE constant,  $\alpha$  is the CPE exponent, and  $R$  refers to the pore resistance or the charge transfer resistance. The measured values of the polarization resistances decreased while the values of the CPE ( $Y^\circ$ ) is raised with increasing the strength of the NaOH solution, denoting the rise in the rate of metal corrosion with raising the strength of the NaOH solution. This is consistent with the results obtained with the other techniques in the present study.

### 3.5. Surface Examination

The scanning electron microscope, SEM, is utilized to examine some of the corroded Al coupons at 25°C. The micrographs depicted in Figs. 9a, 9b demonstrates the surface morphology of the Al metal coupons after inundation (for one hr.) in solutions of 0.05 and 1.0 M NaOH, respectively. Screening of these micrographs discloses the presence of corrosion products deposited on the metal surface that appear

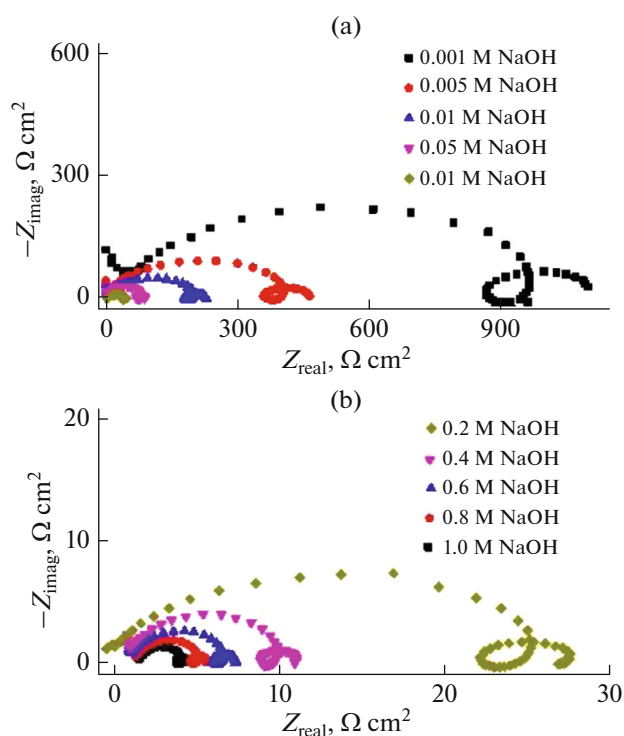


Fig. 7. Nyquist plots for the corrosion of Al electrode in different concentration of NaOH.

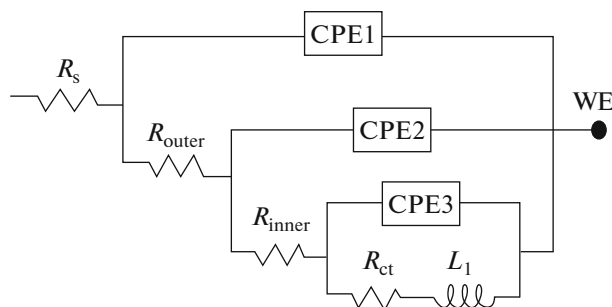


Fig. 8. The equivalent circuit for the impedance data.

denser in 1.0 M NaOH than that shown in 0.05 M solution due to the more destruction effect of the high concentrated NaOH solution confirming the rise in the corrosion rate in the presence of 1.0 M NaOH.

Table 4. Electrochemical polarization parameters, of Al electrode, in 2.0 M NaOH solution at different temperatures

Temperature, K	$-E_{corr}$ , mV/SCE	$I_{corr}$ , mA/cm <sup>2</sup>	$\beta_a$ , mV/SCE	$\beta_c$ , mV/SCE	$R_p$ , $\Omega$ cm <sup>2</sup>
278	1467	21.35	537	412	16.36
288	1469	26.56	399	368	12.19
298	1510	29.38	292	254	08.91
308	1514	34.81	239	216	02.52
318	1520	38.98	187	197	01.70
325	1525	43.95	124	99	01.53

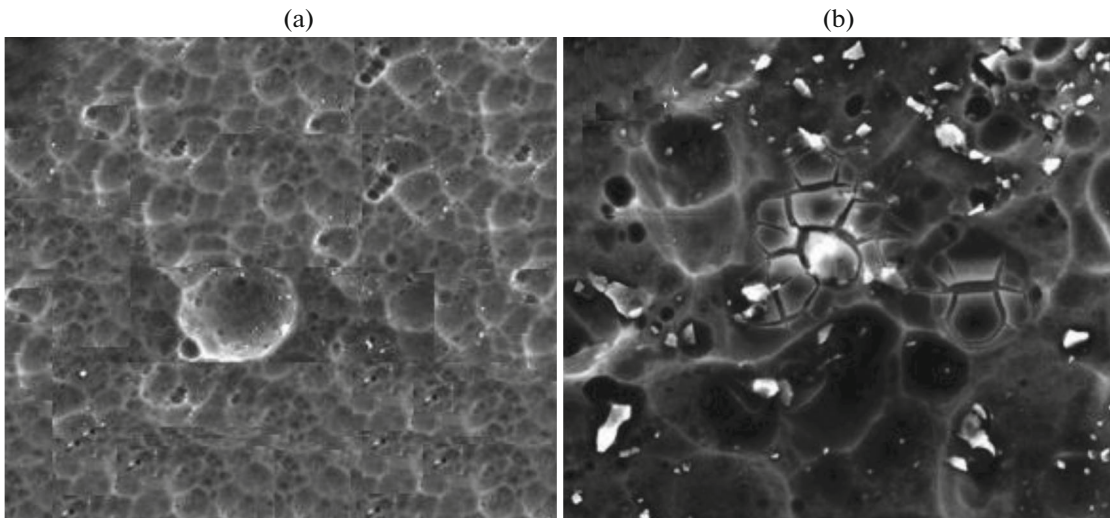


Fig. 9. SEM of Al electrode in (a) 0.05 M NaOH and (b) 1.0 M NaOH, at 25°C.

3.6. Thermodynamic Interpretation

The activation energy of the different processes taking place during the corrosion of Al in NaOH solutions are calculated from the Arrhenius equation [41, 42]. The data of the loss in weight and hydrogen generation techniques could be used to calculate the value of  $E_a$  using the relation:

$$R_{corr} = A \exp(-E_a/RT). \tag{11}$$

However, the data of open-circuit measurement can also be used to calculate the value of  $E_a$  from the relation:

$$\delta^- = A \exp(-E_a/RT), \tag{12}$$

where  $\delta^-$  is the rate of oxide film repair in nm/decade as determined from open circuit potential measurement, A is the Arrhenius constant, R is the universal gas constant, and T is the absolute temperature. The

values of  $\delta^-$  are determined by the application of the direct logarithmic law of oxide film repair and/or destruction. According to this law the OCP, E, (measured till reaching the steady-state potential) as shown in Fig. 2, should vary with the logarithm of inundation time,  $\log t$ , according to a straight-line relationship as seen in Fig. 10 [33, 34, 38, 39]. This figure shows the divergence of the OCP of Al electrode with the  $\log t$ , in 2.0 M NaOH, at different temperatures. From the slope, the rate of  $Al_2O_3$  film destruction  $\delta^-$  could be determined from the relation [41, 42]:

$$E = \text{const} + \frac{2.303\delta^-}{\beta} \log t, \tag{13}$$

where  $\delta^-$  is the rate of oxide film repair in nm/decade, and  $\beta$  is another constant [41, 42].

Arrhenius plots of Al dissolution in 2.0 M NaOH solution as evident from open circuit potential and

Table 5. EIS parameters for corrosion of Al in NaOH solution

$C_{NaOH}$ , M	$R_s$ , $\Omega \text{ cm}^{-2}$	$R_1$ , $\Omega \text{ cm}^{-2}$	$Y_1^\circ \times 10^{-6}$ , $\Omega^{-1} \text{ s}^n \text{ cm}^{-2}$	$n$	$R_2$ , $\Omega \text{ cm}^{-2}$	$Y_2^\circ \times 10^{-6}$ , $\Omega^{-1} \text{ s}^n \text{ cm}^{-2}$	$n$	$R_{ct}$ , $\Omega \text{ cm}^{-2}$	$Y_{ct}, \times 10^{-6}$ , $\Omega^{-1} \text{ s}^n \text{ cm}^{-2}$	$n$	Inductance, $\mu\text{H}$
1.00	1.5	0.48	687.4	0.981	0.76	15.9	0.987	4.4	1.76	0.991	156
0.80	1.4	0.61	453.8	0.977	0.83	12.4	0.981	5.5	1.54	0.989	259
0.60	1.3	0.82	351.1	0.931	0.92	10.9	0.951	7.2	1.37	0.973	386
0.40	1.2	1.09	271.6	0.901	1.3	7.93	0.911	9.7	0.893	0.931	511
0.20	1.0	1.17	253.2	0.866	1.9	6.27	0.886	23.3	0.786	0.899	687
0.10	1.5	1.35	247.4	0.818	2.0	4.93	0.845	46.2	0.513	0.871	740
0.05	2.3	1.89	238.1	0.772	5.4	2.67	0.786	93.7	0.426	0.804	886
0.01	3.9	2.17	217	0.721	6.7	1.48	0.755	209	0.348	0.789	943
0.005	3.8	5.18	187.9	0.691	7.8	0.95	0.708	423	0.256	0.733	1035
0.001	2.9	7.75	165.2	0.629	10.3	0.33	0.688	962	0.186	0.701	1186



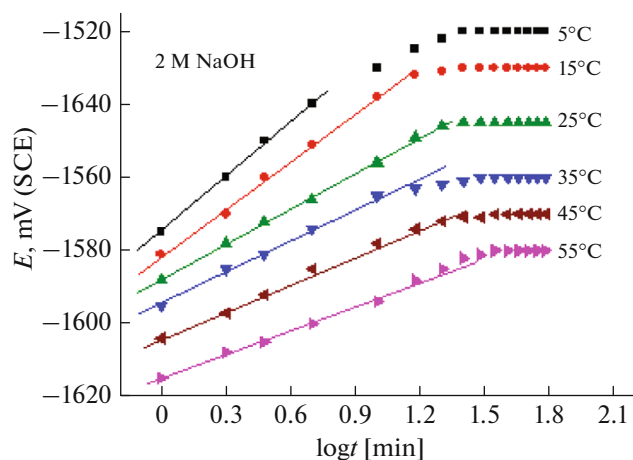


**Fig. 10.** Variation of the open circuit potential of Al electrode with the logarithm of immersion time in 2 M NaOH, at different temperatures.

hydrogen evolution measurements are shown in Figs. 11a, 11b, respectively. Similar plots were obtained using the other experimental techniques (not shown). From Figs. 11a, 11b and the like, the activation energy of the processes occurring during the dissolution of Al in 2.0 M NaOH solutions are computed as indicated in Table 6.

The enthalpy and entropy of activation of  $\text{Al}_2\text{O}_3$  film destruction, metal dissolution, and  $\text{H}_2$  gas generation are calculated according to the transition state theory [58–64]:

$$\delta^- \text{ or } R_{\text{corr}}^- = \frac{RT}{Nh} \exp\left(\frac{\Delta S_a}{R}\right) \exp\left(\frac{-\Delta H_a}{RT}\right), \quad (14)$$

where  $h$  is the Planck's constant, and  $N$  is Avogadro's number. Figures 12a, 12b represents the plots of  $\ln(\delta^-/T)$  and  $\ln(R_{\text{corr}}/T)$  versus  $1/T$  as obtained from open circuit potential and hydrogen evolution data, respectively. Each of  $\Delta H_a$  and  $\Delta S_a$  is calculated, successively, from the values of the slope and intercept of the straight line, Figs. 12a, 12b, as well as from the data obtained from other utilized techniques. The values of energy, enthalpy, and entropy of activation of the destruction of  $\text{Al}_2\text{O}_3$  film, metal dissolution, and hydrogen production on the Al surface, under different experimental conditions, are tabulated in Table 6.

**Table 6.** Thermodynamic activation oxide in solutions, using different techniques parameters for the dissolution of Al

Type of parameter	Technique of measurements			
	open-circuit pot.	weight loss	gasometry	galvostatic
$E_a$ , kJ/mol	10.14	12.54	13.52	10.93
$\Delta H_a$ , kJ/mol	10.27	10.04	11.15	8.30
$\Delta S_a$ , J/mol K	-109	-244	-213	-189

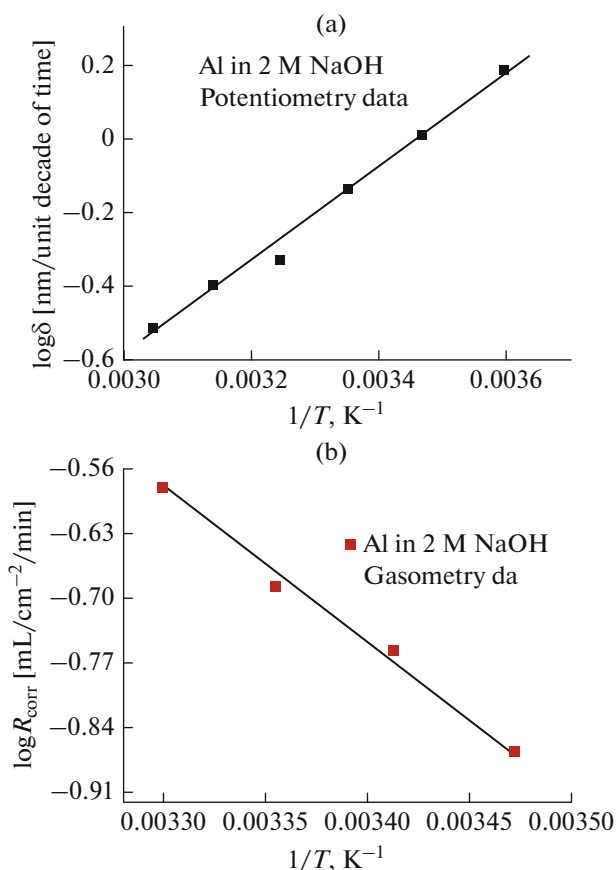


**Fig. 11.** Arrhenius plot of Al in 2 M NaOH solution as evident from (a) open circuit potential and (b) hydrogen evolution measurements.

Analysis of the data presented in this table, which include the thermodynamic functions,  $E_a$ ,  $\Delta H_a$ , and  $\Delta S_a$  for the activation of the destruction of  $\text{Al}_2\text{O}_3$  film, free dissolution of Al, and hydrogen production in 2.0 M NaOH solution, using different chemical and electrochemical techniques, reveals the following:

(i) The values of the activation energy,  $E_a$ , for the electrochemical processes taking place during the dissolution of Al and production of  $\text{H}_2$  gas lie in the range 10.14–13.52 kJ/mol. The low values of  $E_a$  (<40 kJ/mol) indicate that the process of oxide film destruction, the free metal dissolution, and the consequent  $\text{H}_2$  gas production are controlled by a diffusion step [57, 58].

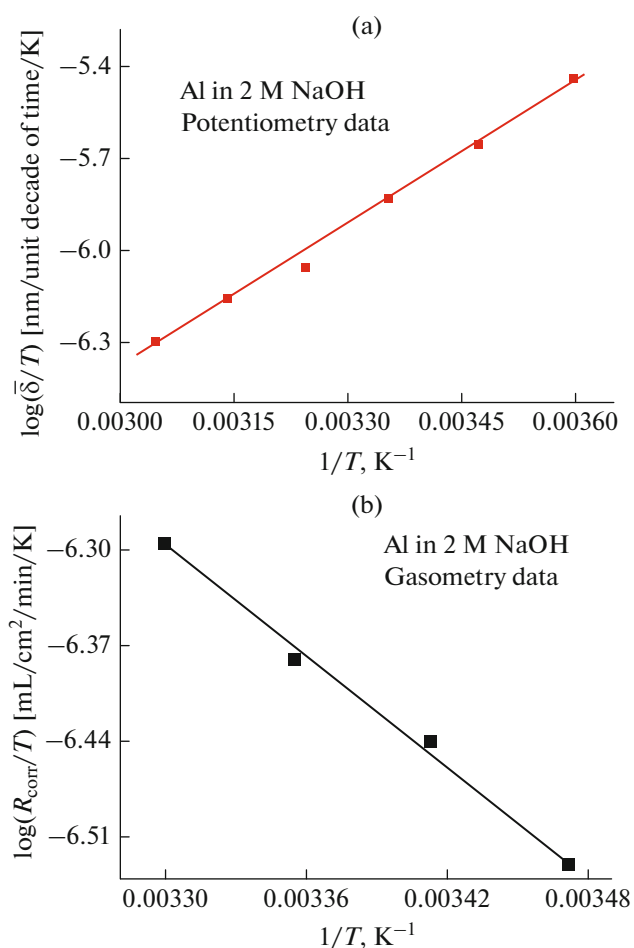


**Fig. 12.** Transition state plots for Al in 2 M NaOH as evident from (a) open circuit potential and (b) hydrogen evolution measurements.

(ii) The positive sign of  $\Delta H_a$  confirms the endothermic nature of the activation transition state complex for all previous processes.

(iii) The negative sign of  $\Delta S_a$  implies that an activation complex is the rate-determining step of oxide film destruction, metal dissolution, and  $H_2$  gas generation. It means that a decrease in the disordering of a dissociation process is taking place [58–61].

(iv) The variance in the values of the thermodynamic functions of Table 6 is supposed to be due to the differences in the experimental techniques used.

## CONCLUSIONS

The dissolution of Al in solutions of different concentrations of NaOH was investigated using the potentiometric, gravimetric, gasometric, galvanostatic polarization, and the EIS techniques, as well as SEM. The obtained data indicate that:

(i) The rates of the processes of  $Al_2O_3$  destruction, dissolution of Al, and hydrogen gas generation in

NaOH solutions depend on solution concentration and temperature.

(ii) The electrochemical parameters,  $E_{corr}$ ,  $i_{corr}$ , and polarization resistance,

$R_p$ , are affected by alkali concentration and temperature.

(iii) The obtained high-frequency capacitive semi-circle confirms a charge transfer reaction at the metal/surface oxide film interface, while the low-frequency capacitive semicircle is due to the dielectric properties of the surface oxide film. The intermediate frequency inductive loop is related to the relaxation process gained by adsorption and incorporation of the  $OH^-$  into the oxide layer.

(iv) The values of activation energies for  $Al_2O_3$  film destruction, aluminum metal dissolution, and hydrogen production are much less than 40 kJ/mol indicating that these processes are controlled by the diffusion step.

(v) The positive sign of  $\Delta H_a$  reflects the endothermic nature of the activation processes taking place during the corrosion of Al in NaOH solutions.

(vi)  $\Delta S_a$  has negative signs indicating a decrease in the disordering of the dissociation processes taken place during Al corrosion and hydrogen gas production.

## CONFLICT OF INTEREST

The authors declare that they have no conflicts of interest.

## REFERENCES

1. Soler, L., Macanas, J., Munoz, M., and Casado, J., *J. Power Sources*, 2007, vol. 169, pp. 144–149.
2. Wang, H., Leung, D.Y.C., Leung, M.K.H., and Ni, M., *Renewable Sustainable Energy Rev.*, 2009, vol. 13, pp. 843–853.
3. Soler, L., Candela, A.M., Macanás, J., Muñoz, M., and Casado, J., *J. Power Sources*, 2009, vol. 192, pp. 21–26.
4. Wang, C., Yu, Y., Niu, J., Liu, Y., Bridges, D., Liu, X., Pooran, J., Zhang, Y., and Hu, A., *Appl. Sci.*, 2019, vol. 9, pp. 1–22.
5. Lædre, S., Kongstein, O.E., Oedegaard, A., Seland, F., and Karoliussen, H., *Int. J. Hydrogen Energy*, 2012, vol. 37, pp. 18537–18546.
6. Hunter, M.S. and Fowle, P., *J. Electrochem. Soc.*, 1956, vol. 103, pp. 482–485.
7. McCafferty, E., *Corros. Sci.*, 2003, vol. 45, pp. 1421–1438.
8. Ying-liang Cheng, Mo-ke Mao, Jin-hui Cao, and Zhao-mei Peng, *Electrochim. Acta*, 2014, vol. 138, pp. 417–429.
9. Abd El Haleem, S.M., Abd El Wanees, S., Abd El Aal, E.E., and Farouk, A., *Corros. Sci.*, 2013, vol. 68, pp. 1–13.
10. Abd El Haleem, S.M., Abd El Wanees, S., Abd El Aal, E.E., and Farouk, A., *Corros. Sci.*, 2013, vol. 68, pp. 14–24.
11. Li, X., Deng, S., and Xie, X., *Corros. Sci.*, 2014, vol. 81, pp. 162–175.

12. Chaubey, N., Singh, V.K., Savita, Quraishi, M. A., and Ebenso, E.E., *Int. J. Electrochem. Sci.*, 2015, vol. 10, pp. 504–518.
13. Adhikari, S. and Hebert, K.R., *Corros. Sci.*, 2008, vol. 50, pp. 1414–1421.
14. Prabhu, D. and Rao, P., *Arabian J. Chem.*, 2017, vol. 10, pp. S2234–S2244.
15. Brown, O.R. and Whitley, J.S., *Electrochim. Acta*, 1987, vol. 32, pp. 545–556.
16. Macdonald, D.D., Lee, K.H., Moccari, A., and Harrington, D., *Corrosion*, 1988, vol. 44, pp. 652–657.
17. Adhikari, S., Lee, J., and Hebert, K.R., *J. Electrochem. Soc.*, 2008, vol. 155, pp. C16–C21.
18. Emregül, K.C. and Aksüt, A.A., *Corros. Sci.*, 2000, vol. 42, pp. 2015–2067.
19. Fan, L., Lu, H., and Leng, J., *Electrochim. Acta*, 2015, vol. 165, pp. 22–28.
20. Elsarrag, E., Elhoweris, A., and Alhorr, Y., *Energy, Sustainability Soc.*, 2017, vol. 7, article no. 9.
21. Zhang, M., Klasky, J., and Letellier, B.C., *J. Nucl. Mater.*, 2009, vol. 384, pp. 175–189.
22. Armstrong, R.D. and Braham, V.J., *Corros. Sci.*, 1996, vol. 38, pp. 1463–1471.
23. Gupta, M., Mishra, J., and Pitre, K.S., *Int. J. Adv. Res. Technol.*, 2014, vol. 5, pp. 50–60.
24. Dražić, D.M., Zečević, S.K., Atanasoski, R.T., and Despić, A.R., *Electrochim. Acta*, 1983, vol. 28, pp. 751–755.
25. Heusler, K.E. and Allgaier, W., *Werkst. Korros.*, 1971, vol. 22, pp. 297–302.
26. Macdonald, D.D., Real, S., Smedley, S.I., and Urquidi-Macdonald, M., *J. Electrochem. Soc.*, 1988, vol. 135, pp. 2410–2414.
27. Perrault, G.G., *J. Electrochem. Soc.*, 1979, vol. 126, pp. 199–204.
28. Radošević, M., Kliškić, J., Dabić, P., Stevanović, R., and Despić, A., *J. Electroanal. Chem.*, 1990, vol. 277, pp. 105–119.
29. Abdel-Gaber, A.M., Khamis, E., Abo-Eldahab, H., and Adeel, Sh., *Mater. Chem. Phys.*, 2010, vol. 124, pp. 773–779.
30. Saleh, M.G.A., Abd El Wanees, S., and Mustafa, S.K., *Chem. Eng. Commun.*, 2019, vol. 206, pp. 789–803.
31. Abd El Wanees, S., El Aal, A.A., and El Aal, E.E., *Br. Corros. J.*, 1993, vol. 28, pp. 222–226.
32. Abd El Wanees, S. and Seda, S.H., *J. Dispersion Sci. Technol.*, 2019, vol. 40, pp. 1813–1826.
33. Abd El Wanees, S., Alahmdi, M.I., Rashwan, S.M., Kamel, M.M., and Abd Elsadek, M.G., *Int. J. Electrochem. Sci.*, 2016, vol. 11, pp. 9265–9281.
34. Abd El Kader, J.M. and Shams El Din, A.M., *Br. Corros. J.*, 1979, vol. 14, pp. 40–45.
35. Solomon, M.M., Umoren, S.A., Udosoro, I.I., and Udoh, A.P., *Corros. Sci.*, 2010, vol. 52, pp. 1317–1325.
36. Evans, U.R., *The Corrosion and Oxidation of Metals*, London: Edward Arnold, 1960, pp. 248–298.
37. El Shayeb, H.A., Abd El Wahab, F.M., and Abd El Meguid, E.A., *Br. Corros. J.*, 2001, vol. 36, pp. 215–220.
38. Abd El Haleem, S.M., Abd El Wanees, S., Abd El Aal, E.E., and Diab, A., *Corros. Sci.*, 2010, vol. 52, pp. 292–302.
39. Abd El Haleem, S.M., Abd El Aal, E.E., Abd El Wanees, S., and Diab, A., *Corros. Sci.*, 2010, vol. 52, pp. 3875–3882.
40. Uhlig, H.H., *Corrosion and Corrosion Control*, New York: John Wiley and Sons, 1971, vol. 381, p. 20.
41. Abd El Haleem, S.M., Abd El Wanees, S., and Bahgat, A., *Corros. Sci.*, 2014, vol. 75, pp. 1–15.
42. Abd El Haleem, S.M., Abd El Wanees, S., and Bahgat, A., *Corros. Sci.*, 2014, vol. 87, pp. 321–333.
43. Zumdahl, S.S., *Chemistry*, D.C. Heath and Co., 1993, p. 645.
44. Abd El Naby, B.A., Khalil, N., and Khamis, E., *Surf. Technol.*, 1984, vol. 22, pp. 367–376.
45. Su-II Pyun and Sung-Mo Moon, *J. Solid State Electrochem.*, 2000, vol. 4, pp. 267–272.
46. Andrew, M.R., *Electrochim. Acta*, 1966, vol. 11, pp. 1425–1436.
47. El Mahdy, G.A. and Mahmoud, S.S., *Corrosion*, 1995, vol. 51, pp. 436–440.
48. Verma, C., Singh, P., Bahadur, I., Ebenso, E.E., and Quraishi, M.A., *J. Mol. Liq.*, 2015, vol. 209, pp. 767–778.
49. Brett, C.M.A., *Corros. Sci.*, 1992, vol. 33, pp. 203–210.
50. Poornima, T., Nayak, J., and Shetty, A.N., *Int. J. Electrochem. Sci.*, 2010, vol. 5, pp. 56–71.
51. Shao, H.B., Wang, J.M., Zhang, Z., Zhang, J.Q., and Cao, C.N., *Mater. Chem. Phys.*, 2003, vol. 77, pp. 305–309.
52. Abdel-Gaber, A.M., Khamis, E., Abo-El Dahab, Sh., and Adeel, H., *Mater. Chem. Phys.*, 2008, vol. 109, pp. 297–305.
53. Lenderink, H.J.W., Linden, M.V.D., and De Wit, J.H.W., *Electrochim. Acta*, 1993, vol. 38, pp. 1989–1992.
54. Morad, M.S., *Mater. Chem. Phys.*, 1999, vol. 60, pp. 188–195.
55. Brett, C.M.A., *J. Appl. Electrochem.*, 1990, vol. 20, pp. 1000–1003.
56. Lorenz, W.J. and Mansfeld, F., *Corros. Sci.*, 1981, vol. 21, pp. 647–672.
57. Keun Lee, K. and Bum Kim, K., *Corros. Sci.*, 2001, vol. 43, pp. 571–575.
58. Badawy, W.A., El-Sherif, R.M., and Shehata, H., *J. Appl. Electrochem.*, 2007, vol. 37, pp. 1099–1106.
59. Wieckowski, A. and Ghali, E., *Electrochim. Acta*, 1985, vol. 30, pp. 1423–1431.
60. Xu, B., Gong, W., Zhang, K., Yang, W., Liu, Y., Yin, X., Shi, H., and Chen, Y., *J. Taiwan Inst. Chem. Eng.*, 2015, vol. 51, pp. 193–200.
61. Abd El Wanees, S., Radwan, A.B., Alsharif, M.A., and Abd El Haleem, S.M., *Mater. Chem. Phys.*, 2017, vol. 190, pp. 79–95.
62. Abd El Wanees, S., Alahmdi, M.I., Alsharif, M.A., and Atef, Y., *Egypt. J. Chem.*, 2019, vol. 26, pp. 811–825.
63. Abd El Wanees, S., Alahmdi, M.I., Abd El Azim, M., and Ahmed, H.E., *Int. J. Electrochem. Sci.*, 2016, vol. 11, pp. 3448–3466.
64. Abd El Wanees, S., Diab, A., Azazy, O., and Abd El Azim, M., *J. Dispersion Electrochem. Sci.*, 2014, vol. 35, pp. 1571–1580.